



**University of
Zurich**^{UZH}

**Zurich Open Repository and
Archive**

University of Zurich
University Library
Strickhofstrasse 39
CH-8057 Zurich
www.zora.uzh.ch

Year: 2016

Soluble oligomers of the pore-forming toxin cytolysin a from escherichia coli are off-pathway products of pore assembly

Roderer, Daniel ; Benke, Stephan ; Schuler, Benjamin ; Glockshuber, Rudi

Abstract: The -pore-forming toxin Cytolysin A (ClyA) is responsible for the hemolytic activity of various *Escherichia coli* and *Salmonella enterica* strains. Soluble ClyA monomers spontaneously assemble into annular dodecameric pore complexes upon contact with membranes or detergent. At ClyA monomer concentrations above 100 nM, the rate-limiting step in detergent- or membrane- induced pore assembly is the unimolecular reaction from the monomer to the assembly-competent protomer, which then oligomerizes rapidly to active pore complexes. In the absence of detergent, ClyA slowly forms soluble oligomers. Here we show that soluble ClyA oligomers cannot form dodecameric pore complexes after the addition of detergent and are hemolytically inactive. In addition, we demonstrate that the natural cysteine pair Cys-87/Cys-285 of ClyA forms a disulfide bond under oxidizing conditions and that both the oxidized and reduced ClyA monomers assemble to active pores via the same pathway in the presence of detergent, in which an unstructured, monomeric intermediate is transiently populated. The results show that the oxidized ClyA monomer assembles to pore complexes about one order of magnitude faster than the reduced monomer because the unstructured intermediate of oxidized ClyA is less stable and dissolves more rapidly than the reduced intermediate. Moreover, we show that oxidized ClyA forms soluble, inactive oligomers in the absence of detergent much faster than the reduced monomer, providing an explanation for several contradictory reports in which oxidized ClyA had been described as inactive.

DOI: <https://doi.org/10.1074/jbc.M115.700757>

Posted at the Zurich Open Repository and Archive, University of Zurich

ZORA URL: <https://doi.org/10.5167/uzh-124849>

Journal Article

Accepted Version

Originally published at:

Roderer, Daniel; Benke, Stephan; Schuler, Benjamin; Glockshuber, Rudi (2016). Soluble oligomers of the pore-forming toxin cytolysin a from *Escherichia coli* are off-pathway products of pore assembly. *Journal of Biological Chemistry*, 291(11):5652-5663.

DOI: <https://doi.org/10.1074/jbc.M115.700757>

Soluble oligomers of the pore-forming toxin Cytolysin A from *Escherichia coli* are off-pathway products of pore assembly

Daniel Roderer^{1,3*}, Stephan Benke², Benjamin Schuler² and Rudi Glockshuber¹

¹ETH Zurich, Institute of Molecular Biology and Biophysics, Otto-Stern-Weg 5, CH-8093
Zurich, Switzerland

²University of Zurich, Department of Biochemistry, Winterthurerstrasse 190, CH-8057 Zurich,
Switzerland

³Present address: Max Planck Institute of Molecular Physiology, Department of Structural
Biochemistry, Otto-Hahn-Strasse 11, D-44227 Dortmund, Germany

*Corresponding author:

Daniel Roderer

Max Planck Institute of Molecular Physiology

Department of Structural Biochemistry

Otto-Hahn-Strasse 11

D-44227 Dortmund, Germany

Phone: (+49)-(0)231-1332312

daniel.roderer@mpi-dortmund.mpg.de

Soluble oligomers of ClyA are off-pathway products of pore assembly.

Keywords: bacterial toxin, Cytolysin A, disulfide bond, redox regulation, protein assembly,
protein conformation, hemolysis

Document Word Count: 9953

Abstract.

The α -pore forming toxin Cytolysin A (ClyA) is responsible for the hemolytic activity of various *Escherichia coli* and *Salmonella enterica* strains. Soluble ClyA monomers spontaneously assemble into annular, dodecameric pore complexes upon contact with membranes or detergent. At ClyA monomer concentrations above ~100 nM, the rate-limiting step in detergent- or membrane- induced pore assembly is the unimolecular reaction from the monomer to the assembly-competent protomer, which then oligomerizes rapidly to active pore complexes. In the absence of detergent, ClyA slowly forms soluble oligomers. Here we show that soluble ClyA oligomers cannot form dodecameric pore complexes after addition of detergent and are hemolytically inactive. In addition, we demonstrate that the natural cysteine pair Cys87-Cys285 of ClyA can form a disulfide bond under oxidizing conditions, and that both the oxidized and reduced ClyA monomers assemble to active pores via the same pathway in the presence of detergent, in which an unstructured, monomeric intermediate is transiently populated. The results

show that the oxidized ClyA monomer assembles to pore complexes about one order of magnitude faster than the reduced monomer because the unstructured intermediate of oxidized ClyA is less stable and dissolves more rapidly than the reduced intermediate. Moreover, we show that oxidized ClyA forms soluble, inactive oligomers in the absence of detergent much faster than the reduced monomer, providing an explanation for several contradictory reports in which oxidized ClyA had been described as inactive.

Introduction.

Pore-forming toxins (PFTs) exist in different orders of bacteria and eukaryotes and cause various human diseases (1). Some of the most potent bacterial toxins are PFTs, such as anthrax toxin (2) and cytolysin from *Vibrio cholerae* (3). A common feature of all PFTs is the conversion from a soluble, monomeric form into a membrane-embedded oligomeric pore complex (1). The membrane-spanning region of the pore can be formed either by α -helices or β -strands; therefore, PFTs are classified as α -PFTs and β -PFTs (4).

The 34 kDa PFT Cytolysin A (ClyA, also termed Hemolysin E (HlyE)) is an α -PFT existing in various *Escherichia coli* and *Salmonella enterica* strains (5-10). The structure of the annular, dodecameric pore complex of *E. coli* ClyA has been solved to atomic resolution (pdb ID 2WCD) (11). The pore subunit (protomer) shows major structural differences when compared to the soluble ClyA monomer (pdb ID 1QOY) (12): The soluble, monomeric form of ClyA consists of a large tail domain with four long α -helices and one short α -helix (α -helices A, B, C, F, and G;

residues 2–159 and 206–303) and a head domain (residues 160–205) with a central, hydrophobic β -hairpin (the “ β -tongue”, residues 185–195) flanked by two short α -helices (α -helices D and E; Figure 1). The tail domain contains a conserved cysteine pair (Cys87 and Cys285 in α -helix B and G, respectively) that can form a disulfide bond (12-14). During pore formation, ClyA undergoes major structural rearrangements involving more than 50% of all amino acids (11). The head domain of the monomer forms elongations of the flanking α -helices (C and F) of the tail domain, and the β -hairpin undergoes a β -to- α transition. The N-terminal α -helix (α A) that is part of the five-helix bundle of the tail domain in the monomer swings around by 180°, elongating the flanking α -helix B and leaving a four-helix bundle in the protomer (Figure 1). The remaining four α -helices of the tail domain rearrange to close the gap left by α A (11). The N-terminal half of α A forms the channel through the target cell membrane. The cysteine pair 87/285 in the reduced protomer remains in spatial proximity with a C_{α} - C_{α} distance of 6.8 Å (Figure 1), which would still enable the formation of a disulfide

bond (15). The formation of the assembly-competent protomer is the rate-limiting step (14) and the prerequisite (16) of pore formation.

Recently, a new study on ClyA activation and pore assembly proposed an alternative mechanism of pore assembly (17): The authors discovered two distinct, homooligomeric species of ClyA that were formed in the absence of detergent or membranes (termed soluble oligomers in the following). These oligomers were interpreted as prepores, similar to soluble, oligomeric intermediates in the pore formation of many β -PFTs (18,19).

Here we examined this alternative pore formation mechanism of ClyA further. We found no evidence for pore formation or efficient target cell lysis when these soluble oligomers were mixed with detergent or horse erythrocytes, respectively. In fact, the soluble ClyA oligomers showed only 1–2% hemolytic activity relative to ClyA monomers. In addition, no pores could be observed by electron microscopy after incubation of soluble oligomers with detergent (n-dodecyl- β -D-maltopyranoside, DDM) under conditions where the majority of ClyA monomers assembled

into dodecameric pore complexes. We therefore interpret the soluble oligomers as off-pathway products of ClyA pore formation. This conclusion is supported by the finding that the kinetics of soluble oligomer formation coincided with loss in hemolytic activity.

In addition, we compared oligomer formation and hemolytic activity of the reduced, dithiol form of ClyA (ClyA_{red}) with pore formation of the oxidized, disulfide form (ClyA_{ox}) in order to address contradictory reports in the literature which had described ClyA_{ox} either as assembly-incompetent and inactive (13,17,20) or as assembly competent (14). In the present study, we show that ClyA_{ox} monomers have essentially the same specific hemolytic activity compared to monomeric ClyA_{red}, but form inactive, soluble oligomers 13–14 times faster than ClyA_{red} upon incubation in the absence of detergent or membranes. The results provide a plausible explanation for previous, contradictory reports on the assembly competence of ClyA_{ox}.

Finally we also investigated the mechanism of the DDM-induced monomer-to-protomer formation of ClyA_{ox} with single molecule Förster resonance

energy transfer measurements and demonstrate that ClyA_{ox} follows the same reaction pathway as ClyA_{red}, in which an unstructured off-pathway intermediate (I_{ox}) is formed (21). Due to the lower stability of I_{ox} compared to I_{red}, assembly-competent protomers are even formed one order of magnitude faster from monomeric ClyA_{ox} compared to monomeric ClyA_{red}.

Materials and Methods.

Materials

Chemicals of highest available purity were purchased from Merck (Germany) or Sigma-Aldrich (Germany). Dithiothreitol (DTT), EDTA and β -mercaptoethanol were obtained from AppliChem (Germany). N-dodecyl- β -D-maltopyranoside (DDM) was purchased from Anatrace (USA). Brain total lipid extract (BTLE) was purchased from Avanti Polar Lipids (USA), and horse erythrocytes were obtained from Oxoid AG (Switzerland).

Production and purification of reduced ClyA

To exclude any influence of an N- or C-terminal polyhistidine purification tag on activity and assembly of ClyA, we introduced a TEV (tobacco etch virus) protease cleavage site between the N-terminal His₆-tag and the natural ClyA sequence into the previously described ClyA expression plasmid derived from pET11a (14). ClyA production in *E. coli* was carried out at 20°C for 15 h as described (16). ClyA was purified from the soluble fraction of the cell extract by Ni²⁺-NTA

affinity chromatography, followed by chromatography on hydroxyapatite as described (14). The N-terminal His₆-tag of ClyA was then cleaved by recombinant, His₆-tagged TEV protease (22), and the resulting wild-type ClyA (residues Thr2–Val 303) was obtained in the flow-through of a second Ni²⁺-NTA affinity chromatography as described (16). All purification steps and the proteolytic cleavage were performed under reducing conditions with buffers containing 2 mM β -mercaptoethanol (when Ni²⁺-NTA columns were used) or 2 mM DTT. The yield of reduced, wild-type ClyA (ClyA_{red}) was 16 mg ClyA per liter of bacterial culture. The concentration of ClyA was determined via its specific absorbance at 280 nm (30370 M⁻¹cm⁻¹ for ClyA_{red}). The ClyA_{red} monomer was stored in PBS buffer (20 mM potassium phosphate pH 7.3, 150 mM NaCl, 0.1 mM EDTA) with 2 mM DTT at 4°C and showed no oligomerization within 7 days.

Preparation and reduction of oxidized ClyA

To generate the disulfide-bonded, oxidized form of ClyA, ClyA_{red} (40 μ M) was incubated in PBS

buffer with 0.5 mM CuCl_2 (i.e. 0.4 mM free CuCl_2) as a catalyst of air oxidation for 3–4 h at 22°C. These conditions guaranteed complete oxidation of the Cys87/Cys285 pair of ClyA (see below). Oxidized ClyA (ClyA_{ox}) was subsequently dialyzed at 4°C against PBS containing 2 mM EDTA and subjected to gel filtration on Superdex 200 (GE Life Sciences, Germany) equilibrated with PBS to separate oxidized monomers from oxidized oligomers. The absence of free thiols in the purified, oxidized monomers was confirmed by Ellman's assay (23) under denaturing conditions (4.0 M guanidinium chloride, pH 8.0) and by analytical reversed-phase HPLC (RP-HPLC) at 30°C on a Zorbax SB300 C8 column (Agilent, USA) using a water-acetonitrile gradient from 50 to 80% (v/v) acetonitrile in 0.1% trifluoroacetic acid (see Figure 2A). The ClyA_{ox} monomer was stored in PBS buffer without DTT at 4°C and showed no oligomerization within 1.5 days.

The reduction of ClyA_{ox} (monomer, oligomer or the assembled pore complex in 0.1% DDM) was performed in PBS with 100 mM DTT (pH 7.3) at 37°C and quantified by RP-HPLC as described

previously (16). Reduction of unfolded ClyA_{ox} was carried out in 50 mM MOPS-NaOH, 4.0 M guanidinium chloride (pH 7.3) with 20 mM DTT at 37°C. Reactions were quenched after different times by addition of formic acid (12% final concentration), and samples were analyzed via RP-HPLC. The peaks corresponding to oxidized and reduced ClyA were integrated, and the data were evaluated according to pseudo-first order kinetics. The reaction between monomeric ClyA_{red} (4 μM) and oxidized DsbA $_{\text{ox}}$ (86 μM , corresponding to the periplasmic DsbA concentration in *E. coli* (24)) at pH 7.3 and 37°C was analyzed in the same way.

Purification and oxidation of FRET donor/acceptor-labeled ClyA for single molecule measurements

A ClyA variant with cysteine residues introduced at positions 56 and 252 (ClyACys) was expressed, purified and labelled at Cys 56 with Alexa Fluor 488 and at Cys 252 with Alexa Fluor 594 as described previously (21). Air oxidation of the natural cysteine pair 87/285 in the labeled ClyACys variant (4 μM) was performed by

incubation in 50 mM $\text{KH}_2\text{PO}_4/\text{K}_2\text{HPO}_4$ pH 7.4, 150 mM NaCl, 10% (v/v) glycerol, 0.5 mM CuCl_2 for 5 h at 22°C. Oligomers formed during this reaction were removed from the monomers by gel filtration on a Superdex 75 10/300 column (GE Healthcare) in PBS. The quantitative formation of the disulfide bond 87-285 was confirmed by reversed phase HPLC on an XTerra RP8 (30 x 4.6 mm) column (Waters) in 0.1% (v/v) trifluoroacetic acid (TFA), using a gradient from 30 to 60% acetonitrile.

Oligomerization of ClyA

Oligomers of reduced or oxidized ClyA were formed in the absence of detergents or lipids by incubation at 37°C (17). For preparative purposes, ClyA_{red} (40 μM) was incubated overnight at 37°C in PBS (pH 7.3) and subsequently subjected to gel filtration (Superdex 200) to separate the oligomer from the remaining monomer. In the case of ClyA_{ox}, 4 h incubation at 22°C (conditions of oxidation of ClyA) resulted in a sufficient amount of oligomeric ClyA (Figure 2A). Kinetics of oligomerization of ClyA_{ox} and ClyA_{red} in PBS at 4°C or 37°C were determined by quantification of

the respective amount of monomeric or oligomeric ClyA via gel filtration on a ProSEC 300S column (Agilent) after different incubation times, starting with 5 μM ClyA monomer. The decrease of the monomer over time was fitted mono-exponentially, assuming a unimolecular rate-limiting step, which is in consistence with previous findings that oligomer formation is concentration-independent at micromolar monomer concentrations (17).

Negative stain transmission electron microscopy

To trigger pore formation from monomers, ClyA (2 μM in PBS) was incubated in 0.1% DDM for 1 h at 22°C. Samples were adsorbed on glow discharged 300 mesh carbon-coated copper grids (Quantifoil, Germany) and negatively stained with 2 mM uranyl acetate. Images were recorded by a KeenView CCD camera using a FEI Morgagni electron microscope operating at an acceleration voltage of 100 kV.

Hemolysis kinetics

Kinetics of ClyA-dependent lysis of horse erythrocytes were measured as described

previously (25) by following the decrease in optical density (OD) at 650 nm using a Varian Cary 100 spectrophotometer (Agilent, USA). Horse erythrocytes at a density of 2×10^6 cells/ml in PBS pH 7.3 were lysed at 37°C by addition of ClyA (final monomer concentrations: 2–100 nM). Reactions with ClyA_{red} additionally contained 2 mM DTT. Hemolysis kinetics were evaluated by linearly fitting the data points in the middle of the lysis reaction between 35 and 75% of the initial optical density. The slope of the linear decrease in optical density was defined as the maximum lysis velocity. The linear dependence of the maximum lysis velocity on the concentration of ClyA was defined as the specific hemolytic activity of the different ClyA species (16).

Circular dichroism (CD) spectroscopy

The monomer-to-protomer transition and pore assembly of ClyA_{ox} and ClyA_{red} (9 μM) in PBS at 22°C was initiated by addition of DDM (final concentration: 0.1% w/v) and followed via the CD signal change at 225 nm using a temperature-controlled J715 CD spectrometer (Jasco, Japan). Samples of reduced ClyA additionally contained

2 mM DTT. Before and after assembly, CD spectra of ClyA_{ox} and ClyA_{red} were recorded. The rate-limiting step of the monomer-to-protomer conversion was fitted according to a first-order reaction.

Single-molecule measurements of ClyA_{ox}

Kinetic single-molecule Foerster resonance energy transfer (FRET) measurements were essentially performed and evaluated as described for the reduced ClyACys variant (21). The measurements were recorded on a modified Micro Time 200 instrument (Picoquant) using a setup for pulsed interleaved excitation (PIE (26)) with two excitation pulses for the donor dye alternating with a single acceptor pulse. The initial phase of protomer formation was measured in a microfluidic mixer (27), and the later phase as well as the pore formation kinetics were constructed from repeated manual mixing measurements (Table 1). All measurements were done at a nominal concentration of labeled ClyACys of 300 pM in PBS with 0.001% (w/v) Tween 20 and 0.1% (w/v) DDM at 22°C. For recording pore formation kinetics with FRET,

excess, unlabeled, oxidized ClyA wt was added at 10 nM or 100 nM to achieve the concentrations required to observe oligomerization of protomers. The model fitting of the protomer formation was performed as described for the reduced variant (21). The three populations in the transfer efficiency histograms were fitted with Gaussian distributions, once with free amplitudes and once with the amplitudes determined by the kinetic model. Due to the extensive overlap of the peaks, the position and width of the monomer peak function were fixed to the values from the first histogram measured in the microfluidic chip and to those of a reference measurement for the microfluidic mixing and manual mixing data, respectively. As the intermediate is not sufficiently populated in the manual mixing experiments, the position and width of the peak function of the intermediate was fixed to those of the fit of the microfluidic mixing data. Uncertainties of the fitted rate coefficients were estimated with a bootstrap analysis on the level of the individual photon bursts. New sets of photon bursts were synthesised by sampling randomly with replacement from the original data. One thousand

synthetic data sets were created, and the resulting histogram time series were fitted as described above. The resulting distributions of the fit parameters are well described by normal distributions.

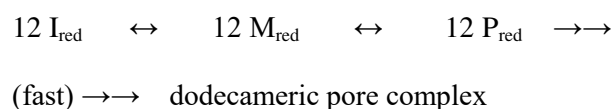
Results.

Soluble ClyA oligomers are formed faster by ClyA_{ox} than by ClyA_{red} and are assembly-incompetent.

Wild-type ClyA contains a single cysteine pair at positions 87 and 285 that is able to form a disulfide bond both in the monomer and in the protomer (14), consistent with the small C_α-C_α distances between the cysteines of 5.2 Å and 6.8 Å in the structures of the monomer and the protomer, respectively (15) (Figure 1). Both ClyA redox forms have been described *in vivo*: Although ClyA lacks an N-terminal signal sequence (28), it is secreted to the periplasm where it accumulates in its oxidized form (20,29). In contrast, assembled ClyA pore complexes that are exported by the bacteria to the extracellular medium in outer membrane vesicles (OMVs) are composed of reduced ClyA protomers (20). The mechanisms underlying the secretion of ClyA into the periplasm and its assembly in OMVs are still unknown.

The DDM-induced assembly of ClyA had been characterized in detail for the disulfide-free form

of ClyA (ClyA_{red}) (21). This study revealed that the unimolecular formation of assembly-competent protomers (P_{red}) from monomers (M_{red}) is rate-limiting for formation of dodecameric pore complexes at concentrations above ~ 100 nM and was accompanied by the reversible formation of a monomeric off-pathway intermediate (I_{red}):



To study the assembly properties of the oxidized form of ClyA (ClyA_{ox}), we first expressed and purified the authentic, untagged ClyA monomer under reducing conditions (2 mM β-mercaptoethanol or DTT) via chromatography of a ClyA variant with N-terminal His₆-tag on Ni²⁺-NTA agarose and chromatography on hydroxyapatite, followed by specific cleavage of the N-terminal His₆-tag by TEV protease. With this procedure, we obtained pure ClyA_{red} (Thr2–Val303), for which Ellman's assay under denaturing conditions confirmed the presence of two thiol groups per polypeptide chain. ClyA_{ox} was obtained from ClyA_{red} after incubation for 4 h with 0.4 mM free CuCl₂ as a catalyst of air

oxidation in PBS buffer (pH 7.3) at 22°C in the absence of detergent. Ellman's assay revealed quantitative formation of the Cys87-Cys285 disulfide bond. This was confirmed by a single peak in reversed-phase HPLC runs, which allows quantitative separation of ClyA_{ox} from ClyA_{red} (Figure 2B).

The preparation of ClyA_{ox} was immediately applied to gel filtration, which revealed three distinct species: The oxidized monomer (M_{ox}), a small (SO_{ox}), and a large (LO_{ox}) oligomer of ClyA_{ox} with apparent molecular masses of 580 and 1180 kDa, respectively (Figure 2A). All three ClyA_{ox} species were isolated and again analyzed for quantitative disulfide bond formation by reversed-phase HPLC (Figure 2B). The analysis confirmed the presence of the disulfide bond in M_{ox}, SO_{ox} and LO_{ox}, and also showed that purified ClyA_{red} stayed completely reduced and proved to be resistant against air oxidation in the absence of Cu²⁺ (Figure 2B).

To test the ability of M_{ox}, SO_{ox} and LO_{ox} to form dodecameric pore complexes, all species were isolated by gel filtration (Figure 2A) and incubated

with 0.1% DDM to trigger pore formation under identical conditions (total monomer concentration of 2 μM, 1 h incubation time, 22°C, pH 7.3). Electron microscopy showed that only M_{ox} readily assembled into pores complexes, while LO_{ox} and SO_{ox} showed no comparable pore formation activity (Figure 2C, top panels).

Next, we found that ClyA_{red} also formed small and large oligomers (SO_{red} and LO_{red}, respectively) in the absence of detergent with the same apparent molecular masses as SO_{ox} and LO_{ox}, but with slower assembly kinetics. Figure 2D shows gel filtration profiles of the kinetics of spontaneous oligomerization of ClyA_{ox} and ClyA_{red} at pH 7.3 and identical initial monomer concentrations of 5 μM, initiated by a temperature shift from 4°C to 37°C. The kinetics of oligomer formation, recorded via the decrease in the peak areas of the monomers, revealed oligomerization half-lives of 60 and 800 min at 37°C for ClyA_{ox} and ClyA_{red}, respectively (Figure 2E and Table 2). Even at 4°C, slow ClyA oligomerization occurred under these conditions, with half-lives of 103 h and 1410 h for ClyA_{ox} and ClyA_{red}, respectively (Table 2). Together, these results show that the spontaneous

formation of the species SO and LO is comparably slow and an intrinsic property of both ClyA redox forms, that ClyA_{ox} oligomerizes about 14 times faster than ClyA_{red} at both 4°C and 37°C, and that oligomerization is strongly favored at the physiological temperature of 37°C. In addition, Figure 2C demonstrates that M_{ox}, in contrast to previous reports describing the inability of ClyA_{ox} to form pores (20) or its lack of cytotoxicity (13,17), readily assembles into annular pore complexes.

Figure 2D shows that the small oligomeric form SO_{red} was much less populated than SO_{ox} during spontaneous oligomerization of ClyA in the absence of detergent, so that we could not separate SO_{red} from the much larger LO_{ox} peak. However, we could isolate LO_{red} by preparative gel filtration. Like LO_{ox}, LO_{red} proved to be assembly-incompetent upon addition of 0.1% DDM, while M_{red} efficiently assembled into pore complexes as shown previously (14,16) (Figure 2C, lower panels). Thus, all oligomeric forms of ClyA that formed in the absence of detergent and could be isolated proved to be assembly-incompetent *in vitro* in the presence of DDM in a time frame

where monomeric ClyA was quantitatively incorporated into pores.

The hemolytic activity of oligomeric forms of oxidized and reduced ClyA is decreased 100-fold relative to the respective monomeric forms.

We next tested the ability of the purified, oligomeric forms LO_{ox}, SO_{ox} and LO_{red} to form active pores in target cells. To this end, we compared their lytic activity towards horse erythrocytes with the hemolytic activity of the monomers M_{ox} and M_{red}. Figure 3A shows hemolysis kinetics at pH 7.3 and 37°C, initiated by mixing erythrocyte suspensions (2×10^6 cells per ml) with LO_{ox}, SO_{ox}, LO_{red}, M_{ox}, or M_{red} at identical total monomer concentrations of 10 nM. The reaction was recorded via the decrease in optical density at 650 nm as a measure of erythrocyte lysis. While M_{ox} and M_{red} proved to be highly active and, after a lag time of about 100 s, caused complete lysis within 200 s, the oligomers LO_{ox}, SO_{ox}, and LO_{red} showed a strongly reduced activity, with lysis half-lives above 2000 s (Figure 3A). For quantification of the specific hemolytic activities of all purified ClyA species, we used the

recently established, linear dependence of the maximum lysis velocity (see Material and Methods for the definition) on ClyA concentration in the range of 1–100 nM ClyA monomer (16). Figure 3B and Table 3 show that freshly prepared M_{ox} and M_{red} showed high specific hemolytic activity, with M_{ox} being even 1.2 times more active than M_{red} ($1.86 \pm 0.14 \text{ mOD s}^{-1} \text{ nM}^{-1}$ and $1.51 \pm 0.07 \text{ mOD s}^{-1} \text{ nM}^{-1}$, respectively). In contrast, the specific activities of the oligomers of ClyA_{red} and ClyA_{ox} were dramatically reduced to 0.9% (LO_{ox} and LO_{red}) and 1.4% (SO_{ox}) of the activity of M_{red} (Figure 3B and Table 3). These results demonstrate that spontaneous formation of ClyA oligomers in the absence of detergent or membranes inhibits formation of active pores in target cells. This provides strong evidence that the species LO and SO of both ClyA redox forms are off-pathway products of pore formation, reminiscent of oligomeric off-pathway species in the α -PFT equinatoxin II from the sea anemone *Actinia equina* (30)) that neither react back rapidly to active monomers, nor integrate into membranes and then become functional pores. The minute hemolytic activity of the oligomers detected in

Figure 3B might result from a very slow dissociation of inactive oligomers to active monomers upon dilution to the low ClyA concentrations (1–100 nM) used in the hemolysis assays.

The high hemolytic activity of M_{ox} contradicts the previously reported assembly incompetence of oxidized ClyA (13,17,20). To test whether the contradictory data in the literature might be caused by the comparably rapid decrease in active monomers in preparations of ClyA_{ox} (Figure 2E), we tested whether the decrease in the concentration of assembly-competent monomers upon oligomerization of ClyA_{ox} and ClyA_{red} coincided with loss of hemolytic activity. For this purpose, ClyA_{ox} and Cly_{red} were again incubated under the conditions described in Figure 2E that favor oligomerization (initial monomer concentration: 5 μM , 37°C, pH 7.3). Samples were taken after different times and analyzed for hemolytic activity as described above. Figure 4 shows the recorded hemolysis profiles and the deduced kinetics of loss of hemolytic activity of ClyA_{ox} and ClyA_{red}, which declined, within a factor of 1.6, with the same half-lives as the

corresponding concentrations of M_{ox} and M_{red} (see Figure 2E, Table 2). At 4°C, the half-lives of hemolytic activity loss of ClyA_{ox} and ClyA_{red} were about 50-fold longer compared to those at 37°C (2.6 days and 16.9 days, respectively, Table 2), showing that storage of ClyA_{ox} at 4°C for two weeks leads to practically complete loss of activity. These results thus provide a plausible explanation for the fact that previous experiments had been interpreted such that ClyA_{ox} is assembly-incompetent (13,17,20).

ClyA_{ox} does not only form annular pore complexes, but even assembles faster than ClyA_{red}.

To identify potential differences in the assembly mechanism of ClyA_{ox} and ClyA_{red}, we first compared the kinetics of the monomer-to-protomer transition and the kinetics of pore formation of ClyA_{ox} and ClyA_{red} in the presence of 0.1% DDM by far-UV CD spectroscopy. In the case of ClyA_{red}, DDM triggered a rapid CD signal intensity increase corresponding to the population of the off-pathway intermediate I_{red}, followed by formation of the protomer P_{red} with more negative CD signal at 225 nm compared to M_{red}, while the

oligomerization of P_{red} to pore complexes remained spectroscopically silent (14). We observed similar, biphasic CD kinetics for ClyA_{ox} at 225 nm (Figure 5A,B). However, the initial increase in the CD signal was less pronounced for ClyA_{ox} (hinting at a lower transient population of the off-pathway intermediate) and the second, rate-limiting step of protomer formation proceeded 7.1 times faster (Figure 5B). The CD spectra and CD kinetics (Figure 5A,B), together with the fact that oxidized and reduced monomers assemble to intact pore complexes in 0.1% DDM (Figure 2C), thus provided a first hint that ClyA_{ox} and ClyA_{red} formed assembly-competent protomers via the same, three-state reaction mechanism ($I \rightleftharpoons M \rightleftharpoons P$) (21), and that ClyA_{ox} formed protomers faster than ClyA_{red}.

To get more quantitative information on the conformational states of ClyA_{ox} populated during DDM-induced protomer formation, we next investigated the kinetics of P_{ox} from M_{ox} by single-molecule FRET experiments as described previously for ClyA_{red} (21). To this end, we used a ClyA_{ox} variant labeled with the FRET pair Alexa488 and Alexa594 at cysteine residues

introduced at position 56 and 252, respectively, showing distinct, conformation-specific transfer efficiencies ($\langle E \rangle$) for M_{ox} , I_{ox} and P_{ox} (21) (Figure 1). We used subnanomolar concentrations of ClyA that prevented protomer assembly, so that only the four unimolecular reactions in the scheme ($I_{ox} \rightleftharpoons M_{ox} \rightleftharpoons P_{ox}$) were observed. The time course of transfer efficiency ($\langle E \rangle$) histograms was fully consistent with the expected conversion of M_{ox} ($\langle E \rangle = 0.42$) to P_{ox} ($\langle E \rangle = 0.67$) with the transient population of the off-pathway intermediate I_{ox} ($\langle E \rangle = 0.20$) (Figure 5C). Compared to ClyA_{red} (21) (dotted lines in Figure 5D), formation of P_{ox} was however about one magnitude faster than P_{red} and virtually completed within 200 s (Figure 5D), and the intermediate I_{ox} was less populated. Compared to I_{red} , which was shown to have molten globule-like characteristics (16,21), I_{ox} showed an increased transfer efficiency ($\langle E \rangle = 0.20$ compared to 0.12 (21), Figure 5C,E) indicating a more compact conformation of I_{ox} in comparison to I_{red} likely due to the covalent linkage of helices B and G by the Cys87-Cys285 disulfide bond. Table 2 compares the microscopic rate constants obtained for the three-state

mechanism of protomer formation of ClyA_{ox} and ClyA_{red}. The results show that the intermediate I_{ox} is 0.5 kJ/mol less stable than M_{ox} , while I_{red} proved to be 4.4 kJ/mol more stable than M_{red} (21). However, P_{ox} was only 4.3 kJ/mol more stable than M_{ox} , while P_{red} is 8.9 kJ/mol more stable than M_{red} (21) (Figure 5F). Overall, ClyA_{ox} formed the protomer 7–8 times faster than ClyA_{red} upon addition of DDM (Figure 5B,D), mainly due to a much lower population of the off-pathway intermediate I (maximum 30% I_{ox} after 10 s, Figure 5D) and, to a smaller extent, due to an about two times faster formation of P from M (Table 2).

Finally, we also compared the kinetics of protomer association and pore assembly of ClyA_{ox} and ClyA_{red} by single-molecule FRET experiments at higher protein concentrations (10 nM) that allowed oligomerization to intact pores. This was achieved by adding an excess of the corresponding, unlabelled ClyA redox form to donor/acceptor labelled ClyA as described previously (21) (see also *Materials and Methods* and legend to Figure 5E for the details). As observed for ClyA_{red} (21), P_{ox} was converted to a state with lower transfer

efficiency ($\langle E \rangle = 0.53$ compared to 0.67 for P_{ox}) representing a mixture, (O_{ox}), of annular pores and emerging, incomplete pores that cannot be distinguished spectroscopically (Figure 5E) (21). These results clearly confirmed the assembly competence of P_{ox} demonstrated by electron microscopy (see Figure 2C) and hemolysis experiments (Figure 3). Moreover, the results showed that assembly of P_{ox} and P_{red} occurred within comparable time frames (Figure 5E). In summary, the single molecule FRET measurements showed that the DDM-induced monomer-to-protomer transition of $ClyA_{ox}$ follows the same kinetic model as observed for $ClyA_{red}$.

The disulfide of $ClyA_{ox}$ is not susceptible to reduction independently of the oligomerization state.

The *in vivo* role of periplasmic $ClyA_{ox}$ has remained enigmatic, in particular because several groups had reported that $ClyA_{ox}$ has a lower intrinsic hemolytic activity than $ClyA_{red}$ (13,17,20). This finding agreed with the observation that strains deficient in the periplasmic dithiol oxidase DsbA, which introduces disulfide

bonds into periplasmic proteins, show $ClyA$ dependent hemolytic activity, while respective wild type strains were hemolytically inactive (20). To investigate the possibility of a regulated change in the $ClyA$ redox state *in vivo*, we tested the accessibility of the disulfide bond of $ClyA_{ox}$ for reduction by DTT. Figure 6A shows that M_{ox} , LO_{ox} , and oxidized pore complexes were reduced only extremely slowly and remained more than 90% oxidized after 3 h even in 100 mM DTT. In contrast, unfolded M_{ox} was completely reduced within 5 min by 20 mM DTT under the same conditions. The deduced rate constants of reduction (see legend to Figure 6A) revealed that the tertiary structure of M_{ox} , LO_{ox} and P_{ox} in pore complexes protected the Cys87-Cys285 disulfide bond 10^5 to 10^6 -fold against reduction relative to unfolded M_{ox} . Reduction of $ClyA_{ox}$ by disulfide exchange at physiologically relevant rates would thus require unfolding, which is also consistent with the inaccessibility to solvent of the 87/285 cysteine pair in the structures of the monomer and protomer (Figure 6C). Finally, we also recorded the kinetics of oxidation of M_{red} by DsbA. This reaction also proved to be extremely slow at

physiological concentrations of DsbA_{ox} (Figure 6B). The results indicate that formation of ClyA_{ox} from folded ClyA_{red} in the periplasm via disulfide exchange with DsbA would require unfolding of M_{red}.

Discussion.

The hemolytic activity and pore formation competence of ClyA_{ox}

In the present study, we addressed two controversies in the literature on the assembly mechanism of ClyA. The first controversy is related to contradictory reports on the ability of ClyA_{ox} to form pore complexes. Several reports suggested that formation of the Cys87-Cys285 disulfide bond in ClyA prevents pore complex formation (13,17,20). A loss of assembly competence of ClyA_{ox} was proposed based on the findings that ClyA in OMVs secreted by cytotoxic *E. coli* strains is present in the reduced form, and that deletion of the periplasmic dithiol oxidase DsbA which oxidizes ClyA in the periplasm restored hemolytic activity (20). In addition, treatment of ClyA with excess Cu(phenantroline)₂, an established reagent for oxidation of cysteine

pairs *in vitro*, led to loss of hemolytic activity that could be partially recovered by treatment with DTT, and a ClyA variant in which both cysteines were replaced by serine residues stayed active independently of the redox conditions (17). Based on these results, it was speculated that formation of the Cys87-Cys285 disulfide prevents the conformational transition to the assembly competent protomers (17). All these data were however in contrast to previous findings that ClyA_{ox} formed active pores upon addition of DDM *in vitro*, and that both ClyA redox forms showed comparable hemolytic activity (14).

We could resolve this controversy with our present study, in which we compared the mechanism of DDM-induced assembly of ClyA_{ox} and ClyA_{red} in detail and in a quantitative manner. The key proved to be the important recent discovery by Fahie *et al.* that ClyA shows a tendency of spontaneous formation of larger oligomers in the absence of detergent, in particular at elevated temperatures (17). We thus compared ClyA_{ox} and ClyA_{red} for their ability of spontaneous oligomer formation. For this purpose, we first established the quantitative absence and presence of the

Cys87-Cys285 disulfide bond in our ClyA preparations (Figure 2B), and we prepared ClyA_{ox} under mild oxidative conditions by using catalytic concentrations of Cu²⁺ ions for Cu²⁺-catalyzed air oxidation. We could fully confirm the formation of two main oligomeric species for ClyA_{red} reported previously (17). In addition, however, we showed that ClyA_{ox} forms soluble oligomer is 13–14 times faster than ClyA_{red}, that oligomer formation is favored at elevated temperatures (Table 2), and that all soluble, oligomeric ClyA forms are hemolytically inactive (see below and Table 3). Thus, formation of assembly incompetent oligomers in preparations of ClyA_{ox} provides a plausible explanation for the interpretations of previous studies that ClyA_{ox} is hemolytically inactive. Specifically, we show that storage of ClyA_{ox} at 4°C for three days already causes a loss of 50% of its hemolytic activity. Therefore, monomers of ClyA_{ox}, freshly isolated from gel filtration chromatography, should be used immediately for assembly studies or kept frozen. We also suggest that ClyA_{red} should be prepared and stored in the presence of reducing agents such as DTT to prevent air oxidation.

We analyzed the kinetic mechanism of DDM-induced pore formation for monomeric ClyA_{ox} and ClyA_{red} in detail, which clearly revealed that ClyA_{ox} is not only fully assembly-competent and forms pores with even 20% higher specific hemolytic activity than pores of ClyA_{red} (Figure 3B), but also follows the same reaction mechanism in which formation of assembly-competent protomers is the rate-limiting step of pore formation at total monomer concentrations above ca. 100 nM, and protomer formation is accompanied by formation of a molten globule-like off-pathway intermediate. Notably, our single molecule FRET experiments showed that the intermediate I_{ox} is less stable than I_{red} and therefore much less populated during protomer formation, so that assembly competent protomers P_{ox} even form about one order of magnitude faster than protomers of ClyA_{red} (P_{red}) (Figure 5). Formation of the Cys87-Cys285 disulfide bridge between the helices B and G thus accelerates protomer formation by decreasing the population of off-pathway intermediates during DDM-triggered pore formation.

ClyA in the periplasm of *E.coli* strains containing DsbA has been reported to be oxidized and to exhibit no cytotoxic activity (13,20). It remains to be established whether ClyA_{ox} also assembles to inactive oligomers in the periplasm, analogous to its spontaneous assembly to oligomers *in vitro*. A recent study reported the co-localization of DsbA and ClyA in OMVs (31), where the reduced form is the main ClyA redox species. Our experiments show that the Cys87/Cys285 pair in folded ClyA_{red} monomers cannot be oxidized efficiently by DsbA (Figure 6B). This makes it unlikely that ClyA_{ox} in OMVs needs to be activated by an unknown reducing agent, as proposed previously (20). An alternative explanation for the presence of ClyA_{red} in OMVs could be that ClyA_{red} is the predominant ClyA species in OMVs because it folds rapidly so that DsbA cannot access the Cys85/Cys285 pair, and that the ClyA molecules that stay in the periplasm are oxidized by molecular oxygen under aerobic conditions. Unraveling the translocation mechanism by which ClyA enters the periplasm in a Sec independent manner appears to be essential for answering this open question.

Are soluble ClyA oligomers really intermediates of an alternative pore formation pathway?

Our previous work (21), together with the present data on the kinetic mechanism of DDM-induced pore formation of ClyA, clearly established a reaction pathway in which the unimolecular formation of protomers from monomers, with the transient population of a molten globule-like off-pathway intermediate, is the rate-limiting step of pore assembly at ClyA concentrations above ca. 100 nM. Here, we also examined the alternative ClyA assembly mechanism proposed by Fahie *et al.* (17), in which soluble ClyA oligomers, formed in the absence of detergent or membranes, represent pre-pores that can integrate into membranes and form hemolytically active pore complexes. We purified soluble oligomers of ClyA_{ox} and ClyA_{red} by gel filtration, but could neither detect a significant population of annular complexes by electron microscopy after addition of detergent (Figure 2C), nor hemolytic activity above 1.4% relative to that of the reduced monomer after mixing the oligomers with erythrocytes (Figure 3B). The interpretation of ClyA oligomers as prepore complexes by Fahie *et*

al. (17) was based on the findings that the oligomers showed hemolytic activity in endpoint hemolysis assays (see below) and single channel conductance activity after reconstitution into planar lipid bilayers. So why did the work of Fahie *et al.* and our present data lead to opposite conclusions on the role of soluble ClyA monomers?

We believe that the main reason for the interpretation by Fahie *et al.* is the fact that the dependence of hemolytic activity of ClyA oligomers on ClyA concentration was not investigated. Erythrocytes were incubated for 15 min at a total ClyA concentration of 0.8 μM , and the amount of hemoglobin released after 15 min by ClyA oligomers and monomers was compared and was used as a measure of hemolytic activity (17). Figure 3 however shows that the amount of lysed cells at a single time point is not a quantitative measure of hemolytic activity. Instead, the hemolytic activity of ClyA can only be quantified accurately via the dependence of maximum lysis velocity (or the inverse lag time of hemolysis (16)) on ClyA concentration (Figure 2B). Therefore, determination of the specific

hemolytic activity of ClyA requires the recording of hemolysis kinetics at different ClyA concentrations. Figure 3A shows that the oligomers LO_{red}, LO_{ox}, and SO_{ox}, already at concentrations of 10 nM, cause significant hemolysis after an incubation time of e.g. one hour although their specific hemolytic activity relative to the monomer is only about 1%. In fact, ClyA monomers are highly active toxins, and incubation of erythrocytes with only 10 nM ClyA monomers leads to complete lysis within 200 s (Figure 3A). The experiments by Fahie *et al.* were however performed at 80-fold higher ClyA concentrations and ClyA activity was deduced from the amount of lysed cells after a single time point (15 min) (17). Figure 3 shows that we would have detected a similar, high hemolytic activity of our purified ClyA oligomers if we had performed our experiments under the same conditions, i.e. at ClyA concentrations of 800 nM.

So what is the reason underlying the low apparent hemolytic activity of ClyA oligomers detected by us and Fahie *et al.*? A rough estimation based on the concentration dependence of ClyA activity (Figure 3B) shows that already a minute fraction

of about 0.1% of monomers spontaneously dissociating from the oligomers and re-assembling into active pores via the classical assembly pathway can readily explain the hemolytic and single channel conductance activity of oligomers detected at the high ClyA oligomer concentrations used by Fahie *et al.* (17). Nevertheless, we cannot completely exclude that ClyA oligomers can react directly to active pores after insertion into erythrocyte membranes, but we believe that this reaction is far too slow for being physiologically relevant.

Acknowledgements.

We thank Hiang Dreher and Helene Fäh-Rechsteiner for excellent technical support, Daniel Nettels for discussion and help with data analysis and Bengt Wunderlich for help in the initial stages of the microfluidic mixing experiments. Electron micrographs were recorded using equipment of the Scientific Center for Optical and Electron Microscopy (SCOPE M) at ETH Zurich. This work was supported by the Swiss National Science Foundation (to R.G. and B.S.) and the National Center of Competence in Structural Biology (to R.G. and B.S.).

Conflict of interest statement

The authors declare that they have no conflicts of interest with the contents of this article

Author contributions.

R.G., D.R. and B.S. designed the research. S.B. and D.R. prepared protein samples and performed the experiments. D.R., S.B., B.S. and R.G. analyzed and interpreted the data. D.R. and R.G. wrote the manuscript with the help of the other authors.

.

References

1. Gonzalez, M. R., Bischofberger, M., Pernot, L., van der Goot, F. G., and Freche, B. (2008) Bacterial pore-forming toxins: the (w)hole story? *Cellular and molecular life sciences : CMLS* **65**, 493-507
2. Blaustein, R. O., Koehler, T. M., Collier, R. J., and Finkelstein, A. (1989) Anthrax toxin: channel-forming activity of protective antigen in planar phospholipid bilayers. *Proc Natl Acad Sci U S A* **86**, 2209-2213
3. Olson, R., and Gouaux, E. (2005) Crystal structure of the *Vibrio cholerae* cytolysin (VCC) pro-toxin and its assembly into a heptameric transmembrane pore. *J Mol Biol* **350**, 997-1016
4. Parker, M. W., and Feil, S. C. (2005) Pore-forming protein toxins: from structure to function. *Prog Biophys Mol Biol* **88**, 91-142
5. del Castillo, F. J., Leal, S. C., Moreno, F., and del Castillo, I. (1997) The *Escherichia coli* K-12 *sheA* gene encodes a 34-kDa secreted haemolysin. *Mol Microbiol* **25**, 107-115
6. Ludwig, A., von Rhein, C., Bauer, S., Huttinger, C., and Goebel, W. (2004) Molecular analysis of cytolysin A (ClyA) in pathogenic *Escherichia coli* strains. *J Bacteriol* **186**, 5311-5320
7. Huang, L. J., Cui, J., Piao, H. H., Hong, Y., Choy, H. E., and Ryu, P. Y. (2010) Molecular cloning and characterization of *clyA* genes in various serotypes of *Salmonella enterica*. *J Microbiol* **48**, 663-667
8. Oscarsson, J., Westermarck, M., Lofdahl, S., Olsen, B., Palmgren, H., Mizunoe, Y., Wai, S. N., and Uhlin, B. E. (2002) Characterization of a pore-forming cytotoxin expressed by *Salmonella enterica* serovars typhi and paratyphi A. *Infect Immun* **70**, 5759-5769

9. von Rhein, C., Hunfeld, K. P., and Ludwig, A. (2006) Serologic evidence for effective production of cytolysin A in *Salmonella enterica* serovars typhi and paratyphi A during human infection. *Infect Immun* **74**, 6505-6508
10. von Rhein, C., Bauer, S., Lopez Sanjurjo, E. J., Benz, R., Goebel, W., and Ludwig, A. (2009) ClyA cytolysin from *Salmonella*: distribution within the genus, regulation of expression by SlyA, and pore-forming characteristics. *International journal of medical microbiology : IJMM* **299**, 21-35
11. Mueller, M., Grauschopf, U., Maier, T., Glockshuber, R., and Ban, N. (2009) The structure of a cytolytic alpha-helical toxin pore reveals its assembly mechanism. *Nature* **459**, 726-730
12. Wallace, A. J., Stillman, T. J., Atkins, A., Jamieson, S. J., Bullough, P. A., Green, J., and Artymiuk, P. J. (2000) *E. coli* hemolysin E (HlyE, ClyA, SheA): X-ray crystal structure of the toxin and observation of membrane pores by electron microscopy. *Cell* **100**, 265-276
13. Atkins, A., Wyborn, N. R., Wallace, A. J., Stillman, T. J., Black, L. K., Fielding, A. B., Hisakado, M., Artymiuk, P. J., and Green, J. (2000) Structure-function relationships of a novel bacterial toxin, hemolysin E. The role of alpha G. *J Biol Chem* **275**, 41150-41155
14. Eifler, N., Vetsch, M., Gregorini, M., Ringler, P., Chami, M., Philippsen, A., Fritz, A., Muller, S. A., Glockshuber, R., Engel, A., and Grauschopf, U. (2006) Cytotoxin ClyA from *Escherichia coli* assembles to a 13-meric pore independent of its redox-state. *EMBO J* **25**, 2652-2661
15. Fass, D. (2012) Disulfide bonding in protein biophysics. *Annual review of biophysics* **41**, 63-79

16. Roderer, D., Benke, S., Muller, M., Fah-Rechsteiner, H., Ban, N., Schuler, B., and Glockshuber, R. (2014) Characterization of Variants of the Pore-Forming Toxin ClyA from *Escherichia coli* Controlled by a Redox Switch. *Biochemistry* **53**, 6357-6369
17. Fahie, M., Romano, F. B., Chisholm, C., Heuck, A. P., Zbinden, M., and Chen, M. (2013) A non-classical assembly pathway of *Escherichia coli* pore-forming toxin cytolysin A. *J Biol Chem* **288**, 31042-31051
18. Degiacomi, M. T., Iacovache, I., Pernot, L., Chami, M., Kudryashev, M., Stahlberg, H., van der Goot, F. G., and Dal Peraro, M. (2013) Molecular assembly of the aerolysin pore reveals a swirling membrane-insertion mechanism. *Nature chemical biology* **9**, 623-629
19. Petosa, C., Collier, R. J., Klimpel, K. R., Leppla, S. H., and Liddington, R. C. (1997) Crystal structure of the anthrax toxin protective antigen. *Nature* **385**, 833-838
20. Wai, S. N., Lindmark, B., Soderblom, T., Takade, A., Westermarck, M., Oscarsson, J., Jass, J., Richter-Dahlfors, A., Mizunoe, Y., and Uhlin, B. E. (2003) Vesicle-mediated export and assembly of pore-forming oligomers of the enterobacterial ClyA cytotoxin. *Cell* **115**, 25-35
21. Benke, S., Roderer, D., Wunderlich, B., Nettels, D., Glockshuber, R., and Schuler, B. (2015) The assembly dynamics of the cytolytic pore toxin ClyA. *Nat Commun* **6**, 6198
22. Finder, V. H., Vodopivec, I., Nitsch, R. M., and Glockshuber, R. (2010) The recombinant amyloid-beta peptide Abeta1-42 aggregates faster and is more neurotoxic than synthetic Abeta1-42. *J Mol Biol* **396**, 9-18
23. Ellman, G. L. (1958) A Colorimetric Method for Determining Low Concentrations of Mercaptans. *Arch Biochem Biophys* **74**, 443-450

24. Crespo, M. D., Puorger, C., Scharer, M. A., Eidam, O., Grutter, M. G., Capitani, G., and Glockshuber, R. (2012) Quality control of disulfide bond formation in pilus subunits by the chaperone FimC. *Nature chemical biology* **8**, 707-713
25. Rennie, R. P., Freer, J. H., and Arbuthnott, J. P. (1974) The kinetics of erythrocyte lysis by *Escherichia coli* haemolysin. *J Med Microbiol* **7**, 189-195
26. Muller, B. K., Zaychikov, E., Brauchle, C., and Lamb, D. C. (2005) Pulsed interleaved excitation. *Biophysical journal* **89**, 3508-3522
27. Wunderlich, B., Nettels, D., Benke, S., Clark, J., Weidner, S., Hofmann, H., Pfeil, S. H., and Schuler, B. (2013) Microfluidic mixer designed for performing single-molecule kinetics with confocal detection on timescales from milliseconds to minutes. *Nature protocols* **8**, 1459-1474
28. del Castillo, F. J., Moreno, F., and del Castillo, I. (2001) Secretion of the *Escherichia coli* K-12 SheA hemolysin is independent of its cytolytic activity. *FEMS Microbiol Lett* **204**, 281-285
29. Ludwig, A., Bauer, S., Benz, R., Bergmann, B., and Goebel, W. (1999) Analysis of the SlyA-controlled expression, subcellular localization and pore-forming activity of a 34 kDa haemolysin (ClyA) from *Escherichia coli* K-12. *Mol Microbiol* **31**, 557-567
30. Rojko, N., Kristan, K. C., Viero, G., Zerovnik, E., Macek, P., Dalla Serra, M., and Anderluh, G. (2013) Membrane Damage by an alpha-Helical Pore-forming Protein, Equinatoxin II, Proceeds through a Succession of Ordered Steps. *J Biol Chem* **288**, 23704-23715

31. Kim, J. Y., Doody, A. M., Chen, D. J., Cremona, G. H., Shuler, M. L., Putnam, D., and DeLisa, M. P. (2008) Engineered bacterial outer membrane vesicles with enhanced functionality. *J Mol Biol* **380**, 51-66
32. Schrodinger, LLC. (2010) The PyMOL Molecular Graphics System, Version 1.3r1.

Abbreviations.

CD	circular dichroism
ClyA	Cytolysin A
ClyA _{ox}	oxidized ClyA with disulfide bond 87-S-S285
ClyA _{red}	reduced ClyA with C87 and C286 in dithiol form
DDM	n-dodecyl- β -D-maltopyranoside
DTT	dithiothreitol
FRET	Förster resonance energy transfer
HPLC	high performance liquid chromatography
I	Intermediate of protomer formation
M	ClyA monomer
O	Soluble ClyA oligomer
OD	optical density
P	ClyA protomer
PBS	phosphate buffered saline
PFT	pore-forming toxin
PIE	pulsed interleaved excitation
RP-HPLC	reversed phase HPLC
TEV	tobacco etch virus

Figure legends.

Figure 1: Ribbon diagrams showing the positions of the natural cysteine residues 87 and 285 in the ClyA monomer (left) and the protomer (middle) in the context of the homododecameric ClyA pore (right). The sulfur atoms of both residues are shown as yellow spheres. Two additional cysteine residues were introduced for site specific labelling with Alexa 488 (green star) at position 56 and Alexa 594 (red star) at position 252 for monitoring the monomer-to-protomer transition by FRET. The FRET efficiencies for both conformational states, calculated based on the respective C_{α} - C_{α} -distances, are indicated. The α -helix G containing Cys285 is colored blue, the segment 81–90 of α -helix B containing Cys87 is depicted in red. The β -tongue of the ClyA monomer and the respective residues in the ClyA protomer are shown in yellow. The figure was prepared with PyMOL (32).

Figure 2: Analysis of spontaneous oligomerization of ClyA_{ox} and ClyA_{red} in the absence of detergent and competence of pore formation of purified ClyA oligomers

A: Preparative gel filtration at pH 7.3 of oxidized ClyA after Cu²⁺-catalyzed air oxidation of ClyA_{red}. Besides the oxidized monomer (M_{ox}), a large (LO_{ox}) and a small (SO_{ox}) oligomeric species could be detected. The apparent molecular masses (in kDa) of LO_{ox} and SO_{ox}, and the masses of calibration standard proteins are indicated. M_{ox} eluted at an apparent molecular mass of 40 kDa.

B: Reversed phase HPLC analysis of ClyA after incubation of ClyA_{red} at pH 7.3 and 22°C for 3.5 h in the presence or absence of 0.4 mM free CuCl₂, showing that ClyA_{red} remained resistant to air oxidation in the absence of CuCl₂, while it was oxidized quantitatively in the presence of CuCl₂. Samples were separated on an analytical C8 column (Agilent) in 0.1% trifluoroacetic acid and eluted with a water/acetonitrile gradient. Due to the denaturing conditions, oligomeric ClyA dissociated so that only a single peak was detected in each run. The HPLC retention times corresponding to ClyA_{red} and ClyA_{ox} are indicated.

C: Negative stain electron micrographs of samples of the purified ClyA_{ox} species LO_{ox}, SO_{ox} and M_{ox} (see. panel A) and the isolated ClyA_{red} species LO_{red} and M_{red} (see panel D) (2 μ M total monomer concentration in each sample) after incubation with 0.1% DDM for 1 h at 22°C. The results show that only M_{ox} and M_{red} were able to form intact pore complexes (Scale bar: 100 nm).

D: Comparison of the spontaneous oligomerization propensity of M_{ox} (black lines) and M_{red} (red lines) (5 μ M each) at 37°C in PBS buffer (pH 7.3). Purified M_{ox} or M_{red} was incubated for zero, 1 h or 5 h at 37 °C, and the reaction products were separated at 22°C in PBS on an Agilent 300S gel filtration column. The results show that M_{ox} has a higher oligomerization tendency than M_{red}, and that both redox species can form large and small oligomers.

E: Kinetics of spontaneous oligomerization of M_{ox} and M_{red} (5 μ M each) at 37°C in PBS buffer (pH 7.3), analyzed via the decrease of the monomer peak. Data were normalized to the initial peak area of the monomer and could be fitted to a first-order decay (solid lines), yielding apparent rate constants of $0.69 \pm 0.02 \text{ h}^{-1}$ for ClyA_{ox} and $0.052 \pm 0.002 \text{ h}^{-1}$ for ClyA_{red}, respectively.

Figure 3: Competence of pore complex formation in the presence of membranes of the different association states of ClyA_{red} and ClyA_{ox}.

A: Hemolytic activity of M, SO and LO at identical total monomer concentrations of 10 nM. The purified species M_{ox}, SO_{ox}, LO_{ox}, M_{red} and LO_{red} (10 nM monomer each) were mixed at 37°C and pH 7.3 with horse erythrocytes (2 x 10⁶ cells per ml). Erythrocyte lysis was followed via the decrease in optical density at 650 nm. Due to its low population, the species SO_{red} could not be purified and separated from LO_{red} by preparative gel filtration. Assays containing reduced ClyA additionally contained 2 mM DTT.

B: Quantification of the specific hemolytic activity of M_{ox}, SO_{ox}, LO_{ox}, M_{red} and LO_{red} via the linear dependence of maximum lysis velocity on ClyA concentration (see Methods and (16) for experimental details), showing that oligomeric species essentially lack hemolytic activity. The maximum lysis velocity (slope of OD₆₅₀ decrease at the half-life of lysis) was plotted against the respective total monomer concentration. The following specific hemolytic activities (in mOD s⁻¹ nM⁻¹) were obtained: M_{ox}: 1.86±0.14; M_{red}: 1.51±0.07; LO_{ox}: 0.013±0.002; LO_{red}: 0.013±0.001; SO_{ox}: 0.021±0.005 (indicated errors represent standard deviations from three independent measurements).

Figure 4: The loss of hemolytic activity of ClyA_{ox} and ClyA_{red} coincides with the decrease in ClyA monomer concentration during spontaneous ClyA oligomerization at 37°C in the absence of detergent or lipids.

A,B: Hemolysis kinetics, initiated by the addition of ClyA_{ox} (A) or ClyA_{red} (B) after different times of oligomerization to horse erythrocytes. The purified monomers M_{ox} and M_{red} were incubated at 37°C and pH 7.3 at a concentration of 5 µM for the indicated time intervals, diluted 500-fold with horse erythrocytes (final concentrations: 2 x 10⁶ cells per ml; 10 nM total monomer concentration), and the decrease in cell density was followed via the decrease in the OD at 650nm.

C: Kinetics of the decrease in hemolytic activity of ClyA_{ox} and ClyA_{red} at 37°C and pH 7.3. The maximum lysis velocity as a measure of hemolytic activity (see Figure 3B) was plotted against incubation time. The decay in hemolytic activity yielded apparent rate constants of 0.53±0.03 h⁻¹ for ClyA_{ox} and 0.085±0.007 h⁻¹ for ClyA_{red}, respectively (solid lines).

Figure 5: Both oxidized and reduced ClyA monomers assemble via the same mechanism into functional pore complexes after addition of the detergent DDM.

A: Far-UV CD spectra of ClyA_{red} and ClyA_{ox} monomers (solid lines) and after assembly to pores in 0.1% DDM at pH 7.3 (dashed lines), demonstrating the increased α-helix content of the protomers in the assembled pore complexes. The total monomer concentration in each sample was 9 µM.

B: Reaction of M_{ox} (grey symbols) and M_{red} (red symbols) to assembly-competent protomers, recorded via the change in the far-UV CD signal at 225 nm. Reactions were initiated by addition of DDM (manual mixing). The gray and red squares represent the CD signals of monomeric $ClyA_{ox}$ and $ClyA_{red}$ in the absence of DDM, respectively. The rate-limiting step of monomer-to-protomer transition was fitted monoexponentially, resulting in apparent rates of protomer formation of $9.64 \pm 0.02 \times 10^{-3} \text{ s}^{-1}$ and $1.35 \pm 0.01 \times 10^{-3} \text{ s}^{-1}$ for $ClyA_{ox}$ and $ClyA_{red}$, respectively.

C,D: Single-molecule FRET measurements of the kinetics of the monomer-to-protomer transition of $ClyA_{ox}$ labelled with Alexa Fluor 488 and 594. Protomer formation was initiated by addition of 0.1% DDM, and the reactions were performed at low ClyA concentrations (300 pM), where oligomerization to pore complexes does not occur (21).

C: Transfer efficiency histograms for the monomer-to-protomer transition of $ClyA_{ox}$ in DDM measured by microfluidics and manual mixing. Each line represents one histogram normalized to a total area of 1. Line colors indicate the reaction time after addition of DDM. The order of the colors is indicated with the bar on the right. I_{ox} : off-pathway intermediate; M_{ox} : monomer; P_{ox} : protomer; r.e.f.: relative event frequency.

D: Time course of the populations of M_{ox} , I_{ox} and P_{ox} after initiation of protomer formation by addition of DDM. Top panel: kinetic model with four rate constants used to fit the kinetic data. Middle panel: sum of squared residuals (SSR) of the kinetic model fit (line) and the free population fit (dots) to the individual histograms. Lower panel: population time courses for M_{ox} , I_{ox} and P_{ox} (blue, green and red squares, respectively), fitted to the model with off-pathway intermediate indicated at the top (solid lines). The dotted lines indicate the previously determined kinetics of protomer formation of $ClyA_{red}$ under identical conditions, fitted to the same reaction mechanism (21).

E: Dependence on ClyA subunit concentration of the kinetics of DDM-induced pore complex formation of $ClyA_{red}$ and $ClyA_{ox}$, recorded by single-molecule FRET experiments. Conditions were identical to those in C and D, but reactions were performed at 10 nM ClyA subunit concentration, allowing oligomerization of assembly-competent protomers and pore complex formation. The higher protein concentrations were achieved by mixing 300 pM FRET-labeled ClyA with excess unlabeled ClyA wt with the same redox state. Emerging and final pore complexes of $ClyA_{ox}$ (left panel) show identical transfer efficiencies of ~ 0.53 and appear as a single peak, $(O_{ox})_n$ (orange), as observed for $ClyA_{red}$ (right panel). The transfer efficiencies of M_{ox} , I_{ox} and P_{ox} (0.42, 0.20 and 0.67, respectively) and M_{red} , I_{red} and P_{red} (21) are also indicated. Transfer efficiency histograms were recorded after different reaction times, with color codes indicated in the bars on the right top of each panel.

F: Schemes of free energies of M, I, and P of $ClyA_{red}$ and $ClyA_{ox}$ in 0.1% DDM at pH 7.3 and 22°C. The free energies of M_{ox} and M_{red} were assumed to be identical. I_{ox} is 0.5 kJ/mol less stable than M_{ox} , while I_{red} is 4.4 kJ/mol more stable than M_{red} . P_{ox} is only 4.3 kJ/mol less stable than M_{ox} , whereas P_{red} is 8.9 kJ/mol more stable than M_{red} .

Figure 6: The natural cysteine pair 87/285 of ClyA is buried and resistant to reduction and oxidation via disulfide exchange.

A: Kinetics of the reduction of M_{ox} , LO_{ox} and assembled pores of $ClyA_{ox}$ by 100 mM DTT at 37°C, pH 7.3 and identical total monomer concentrations of 5 μ M (the reaction with assembled pores also contained 0.1% DDM). As a control, unfolded ClyA in 4 M guanidinium chloride was reduced at 37°C and pH 7.3 with 20 mM DTT. The reactions were stopped after different times by addition of formic acid (16% final concentration), and oxidized and reduced ClyA were analyzed via RP-HPLC (see Figure 2B). The decrease in the fraction of $ClyA_{ox}$ was fitted according to a pseudo first-order reaction, resulting in rate constants of $1.1 \pm 0.1 \text{ M}^{-1} \text{ s}^{-1}$ for unfolded ClyA, $1.9 \pm 1.1 \times 10^{-5} \text{ M}^{-1} \text{ s}^{-1}$ M_{ox} , $1.2 \pm 0.2 \times 10^{-5} \text{ M}^{-1} \text{ s}^{-1}$ for LO_{ox} , and $1.9 \pm 0.2 \times 10^{-6} \text{ M}^{-1} \text{ s}^{-1}$ for the oxidized ClyA pore complex.

B: Oxidation of monomeric $ClyA_{red}$ (5 μ M) by 86 μ M $DsbA_{ox}$ (*in vivo* concentration in *E. coli* (24)) at 37°C and pH 7.3. The decrease in the fraction of $ClyA_{red}$ was fitted according to a pseudo first-order kinetics, yielding a rate constant of $4.3 \pm 0.1 \times 10^{-2} \text{ M}^{-1} \text{ s}^{-1}$ for the oxidation of $ClyA_{red}$ by $DsbA_{ox}$.

C: Semi-transparent surface representation of the ClyA monomer (left) and the ClyA protomer (right) in the region around the cysteine pair 87/285, showing that the sulfur atoms of Cys87 and Cy285 are buried in both structures. The positions of α -helices B (red) and G (blue) and the C-termini are indicated. The sulfur atoms of Cys87 and Cys285 are shown as yellow spheres. The figure was illustrated in PyMOL (32).

Tables.**Table 1:** Single-molecule FRET datasets collected for the kinetic analysis for ClyA protomer and pore formation. Repeats used: number of measurements taken for the specified time, Time window length: size of time windows the cumulated measurements were divided into, Burst min/max: lower and upper limit of number of photons in a burst to be considered for the analysis, NA: not applicable.

Total ClyA concentration	Total measurement time	Repeats used	Time window length	Burst min/max
100 pM	60 sec (microfluidics)	NA	NA	40/300
100 pM	10 min	21	60 s	80/250
100 pM	30 min	9	180 s	80/250
100 pM	60 min	2	900 s	80/250
10 nM	15 min	8	30 s	80/250
10 nM	60 min	4	300 s	80/250
100 nM	5 min	24	30 s	80/250
100 nM	15 min	13	60 s	80/250
100 nM	30 min	4	300 s	80/250
100 nM	60 min	2	600 s	80/250

Table 2: Apparent rate constants of the decay of hemolytic activity of M_{red} and M_{ox} as a consequence of spontaneous oligomerization in PBS in the absence of detergent or membranes, recorded at identical initial monomer concentrations of 5 μ M.

	$ClyA_{red}$	$ClyA_{ox}$
Decrease of hemolytic activities and monomer depletion		
Decrease of hemolytic activity at 37 °C (h^{-1})^(a)	$8.5 \pm 0.7 \cdot 10^{-2}$	$5.3 \pm 0.3 \cdot 10^{-1}$
Monomer depletion at 37 °C (h^{-1})^(b)	$5.2 \pm 0.2 \cdot 10^{-2}$	$6.9 \pm 0.2 \cdot 10^{-1}$
Decrease in hemolytic activity at 4 °C (h^{-1})^(c)	$1.7 \pm 0.1 \cdot 10^{-3}$	$1.1 \pm 0.1 \cdot 10^{-2}$
Monomer depletion at 4 °C (h^{-1})^(c)	$4.9 \pm 0.5 \cdot 10^{-4}$	$6.7 \pm 0.2 \cdot 10^{-3}$
Kinetics of $I \leftrightarrow M \leftrightarrow P$, determined by single molecule FRET		
k_{MI} at 22 °C in DDM (s^{-1})	$3.0 \pm 0.3 \cdot 10^{-1}$ ^(d)	$1.2 \pm 0.1 \cdot 10^{-1}$ ^(e)
k_{IM} at 22 °C in DDM (s^{-1})	$5.0 \pm 1.0 \cdot 10^{-2}$ ^(d)	$1.5 \pm 0.1 \cdot 10^{-1}$ ^(e)
k_{MP} at 22 °C in DDM (s^{-1})	$1.7 \pm 0.6 \cdot 10^{-2}$ ^(d)	$4.7 \pm 0.3 \cdot 10^{-2}$ ^(e)
k_{PM} at 22 °C in DDM (s^{-1})	$4.7 \pm 0.5 \cdot 10^{-4}$ ^(d)	$8.1 \pm 0.2 \cdot 10^{-3}$ ^(e)

(a): see Figure 4 C

(b): see Figure 2 E

(c): data not shown

(d): Benke *et al.* (21)

(e): rate constants obtained by single molecule FRET (Figure 5D)

Table 3: Specific hemolytic activities of the different forms of oxidized and reduced ClyA.

	specific hemolytic activity at 37°C (mOD s⁻¹ nM⁻¹)	% of specific activity of M_{red}
reduced, monomer	1.51±0.07	100
oxidized, monomer	1.86±0.14	123
reduced, large oligomer	0.013±0.001	0.9
oxidized, large oligomer	0.013±0.002	0.9
oxidized, small oligomer	0.021±0.005	1.4

Figure 1

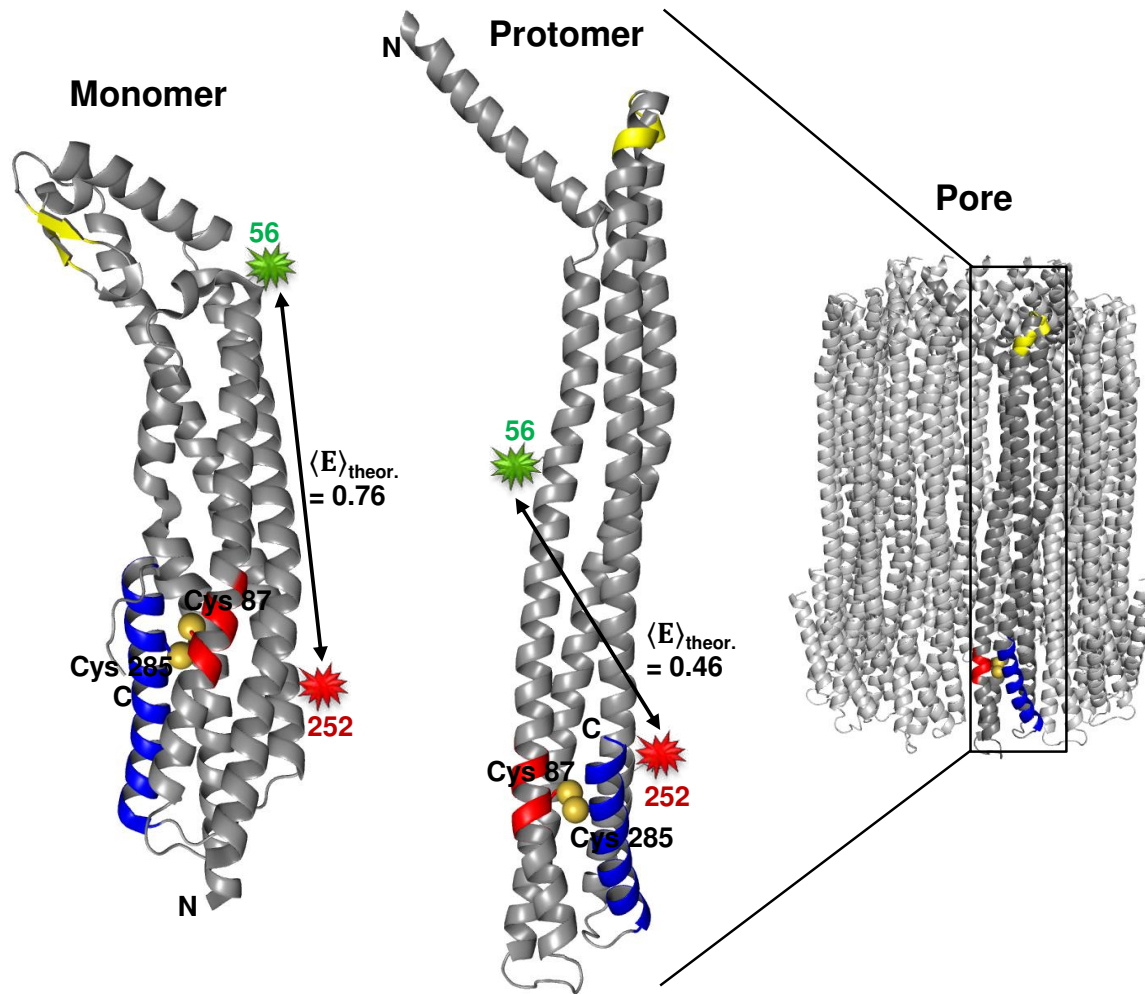


Figure 2

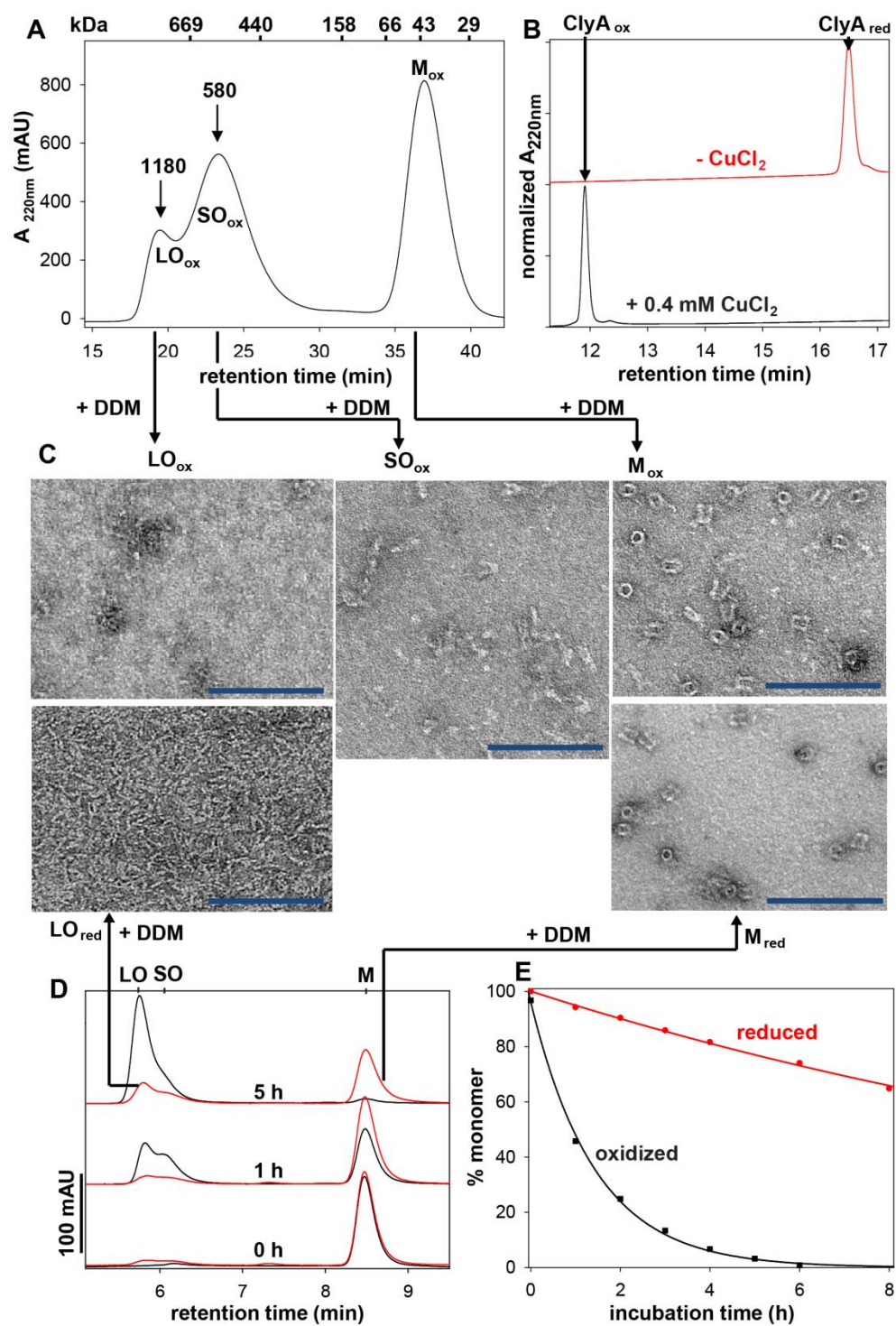


Figure 3

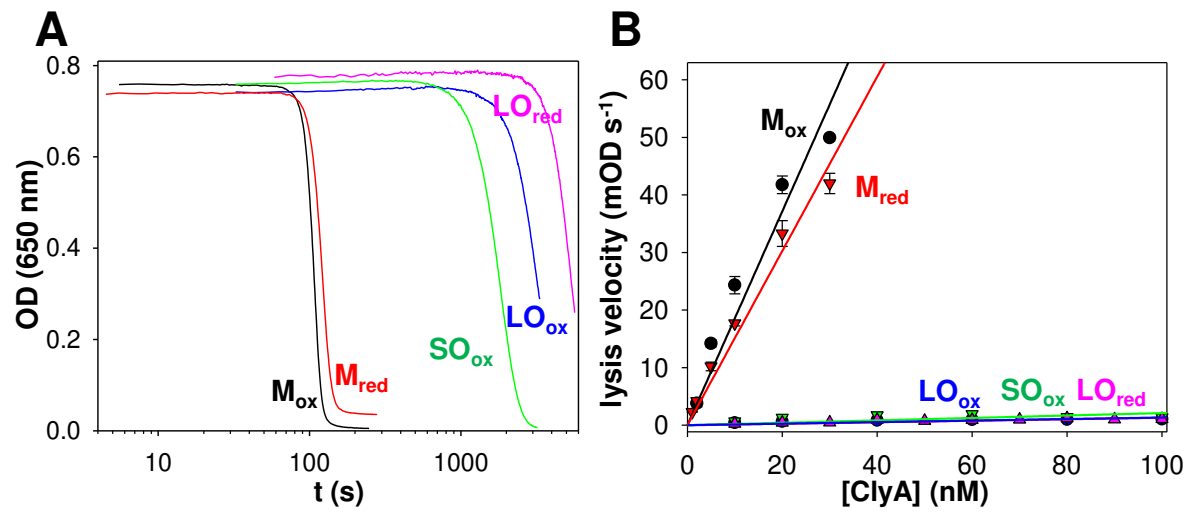


Figure 4

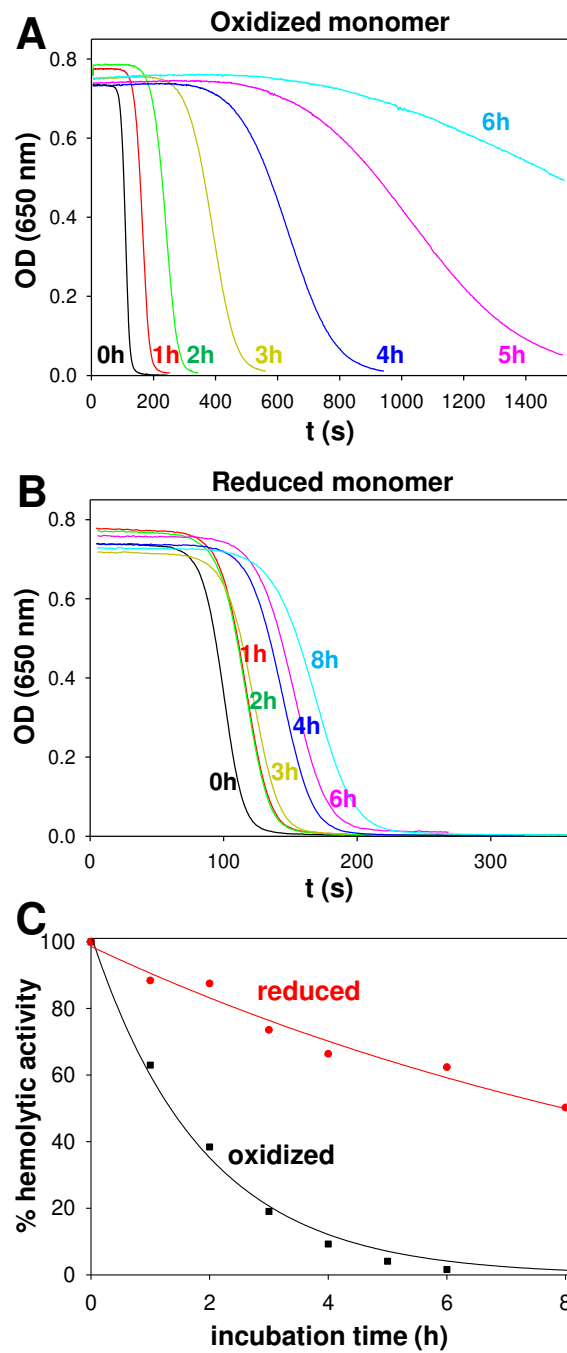


Figure 5

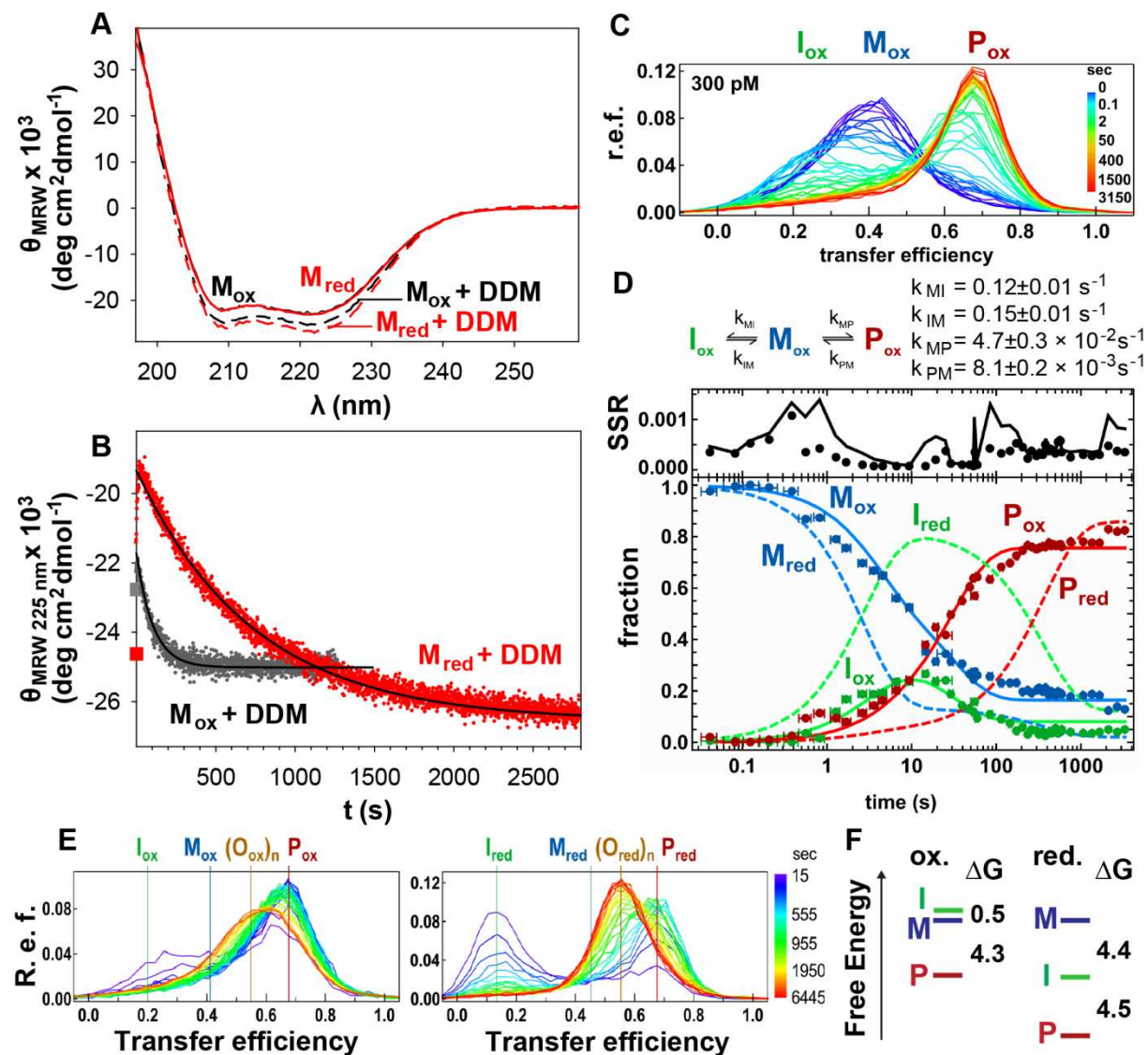
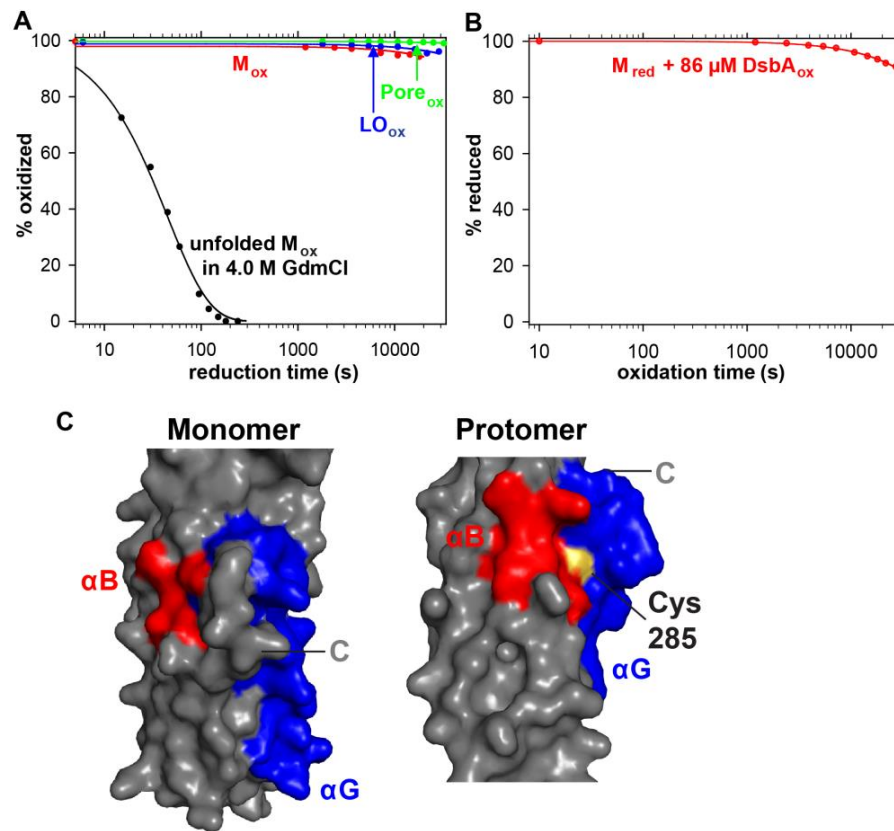


Figure 6



Soluble oligomers of the pore-forming toxin Cytolysin A from Escherichia coli are off-pathway products of pore assembly

Daniel Roderer, Stephan Benke, Benjamin Schuler and Rudi Glockshuber

J. Biol. Chem. published online January 12, 2016

Access the most updated version of this article at doi: [10.1074/jbc.M115.700757](https://doi.org/10.1074/jbc.M115.700757)

Alerts:

- [When this article is cited](#)
- [When a correction for this article is posted](#)

[Click here](#) to choose from all of JBC's e-mail alerts

This article cites 0 references, 0 of which can be accessed free at
<http://www.jbc.org/content/early/2016/01/12/jbc.M115.700757.full.html#ref-list-1>